

Numerical Evaluation of the Image Space Reconstruction Algorithm

Tomohiro Aoyagi^a and Kouichi Ohtsubo

Faculty of Information Science and Arts, Toyo University, 2100 Kujirai, Saitama, Japan

Keywords: X-ray CT, PET, Image Reconstruction, ISRA, Steepest Descent.

Abstract: In medical imaging modality, such as X-ray computerized tomography (CT), positron emission tomography (PET) and single photon emission computed tomography (SPECT), image reconstruction from projection is to produce an image of a two-dimensional object from estimates of its line integrals along a finite number of lines of known locations. The method of tomographic image reconstruction from projection can be formulated with the Fredholm integral equation of the first kind, mathematically. It is necessary to solve the equation. But it is difficult in general to seek the strict solution. By discretizing the image reconstruction problem, we applied the image space reconstruction algorithm (ISRA) to the problem and evaluated the image quality. We computed the normalized mean square error (NMSE) in reconstructed image. We have shown that the error decreases with increasing the number of detectors, views and iterations. In addition, the effect of the relaxation parameter, the weighting factor and the noise to the reconstructed image are analysed.

1 INTRODUCTION

In medical imaging modality, such as X-ray computerized tomography (CT), positron emission tomography (PET) and single photon emission computed tomography (SPECT), image reconstruction from projection is to produce an image of a two-dimensional object from estimates of its line integrals along a finite number of lines of known locations (Herman, 2009; Kak et al., 1998; Imiya, 1985). PET or SPECT is intrinsically a three-dimensional imaging technique and determines the distribution of a radiopharmaceutical in the interior of an object by measuring the radiation outside the object in a tomographic fashion (Bendriem et al., 1998). The method of tomographic image reconstruction from projection can be formulated by the Fredholm integral equation of the first kind, mathematically. Since observed data can be discretized experimentally, it is necessary to discretize the equation to solve it with digital processing. Because of the ill-posed nature, it is difficult to solve strictly this integral equation. Up to now many image reconstruction methods have been proposed by the research development regardless of imaging modality (Stark, 1987; Natterer et al., 2001). In general inverse problems, the regularization of

linear ill-posed problems has been derived and revealed the properties (Daniel 2021; Ronny et al., 2019; Simon et al., 2022).

It is possible to divide image reconstruction methods into two methods, transform and iterative.

Transform methods are based on discrete implementations of analytic solution and give a one-step solution which is directly calculated from the observed data. Iterative method can incorporate the discrete nature of the data sampling and reconstruction problem and typically some statistical model of the data acquisition process.

The image space reconstruction algorithm (ISRA) which is one of the iterative algebraic reconstruction methods, has been shown to be a non-negative least squares estimator and was introduced as an alternative image reconstruction method for PET (Depierro, 1987; Iniyatharasi et al., 2015). By modifying the weighted least squares objective function, a more general form of the ISRA has been derived and the relation between ISRA and the maximum likelihood expectation maximization (MLEM) has been revealed and shown the convergence property (Depierro, 1993; Reader, 2011).

However, the effect of discretizing an image reconstruction model and its parameter have been not revealed sufficiently. In this paper, by discretizing the


^a <https://orcid.org/0000-0002-7268-9826>

image reconstruction problem, we applied ISRA to the problem and evaluated the image quality. We computed the normalized mean square error (NMSE) in reconstructed image. We have shown that the error decreases with increasing the number of detectors, views and iterations. By introducing the new weighting factors which is the linear combination of the expected data vector from a given image estimate, measured data vector and constant term, new update method was derived. Also, we have shown the effect of the relaxation parameter and noise to the reconstructed image.

2 REVIEW OF ISRA

The observed data $\mathbf{g}=\{g_i\}_{i=1}^N$ can be viewed as the components of a vector which will be called the data vector or an element in the finite dimensional Hilbert space. The unknown characteristics of the sample, denoted by $\mathbf{f}=\{f_j\}_{j=1}^M$, can be called the object of its physical nature. Image reconstruction problems or imaging system models can be formulated by using the matrix notation (Bertero et al., 1985; Bertero et al., 1988).

$$\mathbf{g}=\mathbf{A}\mathbf{f} \quad (1)$$

The linear operator \mathbf{A} is an $N \times M$ real matrix $\mathbf{A} = \{a_{ij}\}$.

Let us consider the following weighted least-squares objective function, such that,

$$\Phi_{obj}(\mathbf{f}^k) = \frac{1}{2} \sum_{i=1}^N \frac{(g_i - p_i^k)^2}{w_i}, \quad (2)$$

where the estimated data from a given image estimate \mathbf{f}^k are given by

$$p_i^k = \sum_{j=1}^M a_{ij} f_j^k + \alpha_i. \quad (3)$$

α_i can be of signal-independent noise. Now, we seek a better estimate of \mathbf{f} , which reduces the evaluation of the objective function or satisfies the minimum of the objective function. This can be achieved by taking partial derivatives with respect to \mathbf{f} .

$$\frac{\partial}{\partial f_j^k} \Phi_{obj}(\mathbf{f}^k) = - \sum_{i=1}^N \frac{a_{ij}(g_i - p_i^k)}{w_i}. \quad (4)$$

The right-hand side of eq. (4) can be of an image which is the backprojection of weighted expected

data minus the backprojection of the weighted projection data.

$$\frac{\partial}{\partial f_j^k} \Phi_{obj}(\mathbf{f}^k) = \sum_{i=1}^N a_{ij} \frac{p_i^k}{w_i} - \sum_{i=1}^N a_{ij} \frac{g_i}{w_i} \quad (5)$$

The general iteration scheme to minimize the objective function (2) can be derived by subtracting a variably-scaled amount of this gradient image.

$$f_j^{k+1} = f_j^k - \beta_j^k \left(\sum_{i=1}^N a_{ij} \frac{p_i^k}{w_i} - \sum_{i=1}^N a_{ij} \frac{g_i}{w_i} \right) \quad (6)$$

This is the same method of steepest descent which is the most widely used descent procedure for minimizing an objective function (Luenberger, 1969; Luenberger, 2003). If the following scaling is chosen for a given iteration k ,

$$\beta_j^k = \frac{f_j^k}{\sum_{i=1}^N a_{ij} \frac{p_i^k}{w_i}}, \quad (7)$$

the iterative update can be obtained.

$$f_j^{k+1} = f_j^k \frac{\sum_{i=1}^N a_{ij} \frac{g_i}{w_i}}{\sum_{i=1}^N a_{ij} \frac{p_i^k}{w_i}}. \quad (8)$$

Moreover, if the weights are chosen to be $w_i = 1$, then ISRA can be obtained, such that,

$$f_j^{k+1} = f_j^k \times \frac{\sum_{i=1}^N a_{ij} g_i}{\sum_{i=1}^N a_{ij} \langle \mathbf{a}^i, \mathbf{f}^k \rangle} \quad (9)$$

where $\langle \cdot, \cdot \rangle$ indicates the inner products in Hilbert space.

3 NUMERICAL COMPUTATIONS

3.1 Discretization of Image Reconstruction Problem

To confirm the effectiveness of the method, computer simulations have been carried out. A Cartesian grid of the square observation plane, called pixels, is introduced into the region of interest (ROI) so that it covers the whole observation plane that has to be reconstructed. The pixel as numbered as follows: the top left corner pixel is set to 1 and bottom right corner is numbered as M with Raster scanning. The object to be reconstructed is approximated to the one that takes a constant uniform value f_j throughout the j -th pixel, for $j = 1, 2, \dots, M$. Consequently, the vector $\mathbf{f} =$

$\{f_j\}_{j=1}^M$ in \mathbb{R}^M (the m -dimensional Euclidean space) is the discretized version of the object (Censor et al., 2008). For our simulations we assumed the fan beam scanner in data collection mode. It consists of a single source and multiple detectors combination which rotates around ROI. The detector-array can be discretized equidistantly. The set of all lines for which line integrals are estimated can be divided into D lines in each combination. We assumed projection angle $\theta = [0, 2\pi[$, and it is discretized at even. The total number of the angles is V . It means the number of views per 360° . The total number of all discretized line is N , which define the line of response (LOR), such that,

$$N = D \times V. \quad (10)$$

We set the left detector element to 1 at $\theta = 0$ and the right detector element to N at last View. Thus i indicates any detector elements and $i = 1, 2, \dots, N$. Consequently, the vector $\mathbf{g} = \{g_i\}_{i=1}^N$ in \mathbb{R}^N is the discretized version of the line integrals. We denote the length of intersection of the i -th line with the j -th pixel by a_j^i , for all $i = 1, 2, \dots, N$, $j = 1, 2, \dots, M$. Figure 1 shows the discretized model of the image reconstruction problem.

The ISRA is the following iterative scheme.

Algorithm.

Step 1 (Initialization): $\mathbf{f}^0 \in \mathbb{R}^M \setminus \{0\}$.

Step 2: Compute the backprojection of projection data.

$$\mathbf{h}_j = \sum_{i=1}^N a_{ij} \mathbf{g}_i. \quad (11)$$

Step 3 (Iterative step): Given \mathbf{f}^k and fixed the relaxation parameter γ_j , compute

$$\mathbf{f}_j^{k+1} = \mathbf{f}_j^k \times \left(\frac{\mathbf{h}_j}{\sum_{i=1}^N a_{ij} \langle \mathbf{a}^i, \mathbf{f}^k \rangle} \right)^{\gamma_j}. \quad (12)$$

3.2 Text Based Phantom

Our first image is a text based phantom. Figure 2 shows its original test image 1, discretized 128×128 pixels and 8 bit/pixel. Figure 3 shows the projection data of the original test image 1. The number of detectors per view is 200. The number of views per 360° is 200. Figure 4 shows the reconstructed images by ISRA. In this case, iteration number is 30. The number of detectors per view is 200. The number of views per 360° is 200. Initial data is a uniform image of 0.1, $0.1 = \mathbf{f}^0 \in \mathbb{R}^M$. The relaxation parameter is the unit.

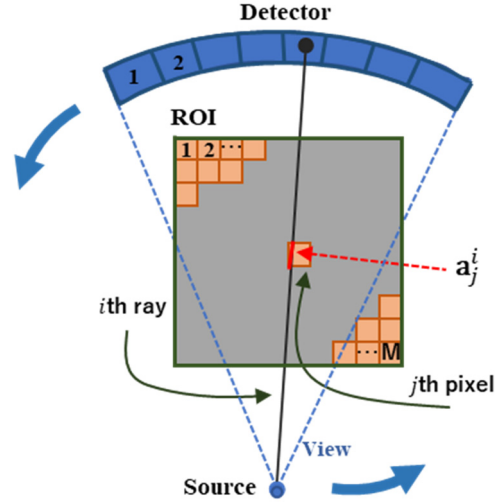


Figure 1: The fully-discretized model of the image reconstruction problem in 2-dimensional space. Fan beam scanning mode (single source, multiple detector, translate-rotate).



Figure 2: The original test image 1 (128×128 pixels, 8bpp).

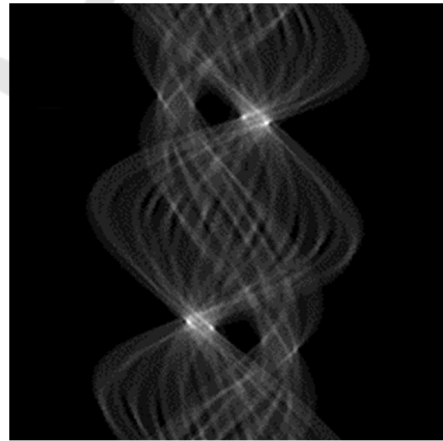


Figure 3: The projection data, Sinogram of the original image in Fig. 2. 200 detectors / view, 200 views / 2π and 8bpp. Noise free.



Figure 4: The reconstructed image by ISRA after 30 iterations. Initial image is a uniform image of 0.1. The relaxation parameter $\gamma_j = 1.0$.

To confirm the effect of number of detectors per view, we computed the reconstructed image with its variations from 100 to 250. Figure 5 illustrates the plots of the normalized mean square error versus iteration number. In this case, we set the number of views per 360° equal to 200 and the relaxation parameter the unit. Initial data is a uniform image of 0.1, $0.1 = \mathbf{f}^0 \in \mathbb{R}^M$. Iteration number is up to 30. The normalized mean square error (NMSE) is defined by

$$\text{NMSE}(k) = \frac{\|\mathbf{f}^k - \mathbf{f}\|_2}{\|\mathbf{f}\|_2}, \quad (13)$$

where \mathbf{f}^k is the image after k 'th iteration step and \mathbf{f} is the original image. $\|\cdot\|_2$ indicates the ℓ^2 -norm. From Fig. 5 we can see that the error decreases with increasing the number of iterations and the error decreases as a whole with increasing the number of detectors.

To confirm the effect of number of views per 360° , we computed the reconstructed image with its variations from 50 to 200.

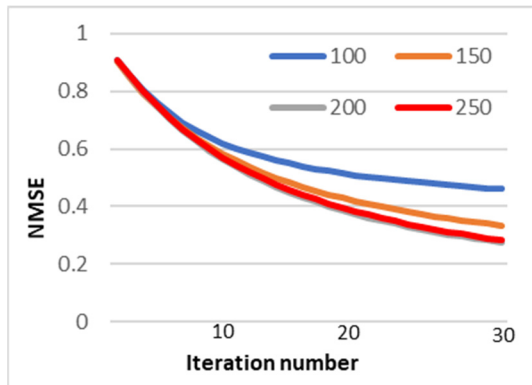


Figure 5: Plots of normalized mean square error versus iteration number. 200 views. Initial image is a uniform image of 1.0. Relaxation parameter is the unit. The number of detectors / view are changed from 100 to 250.

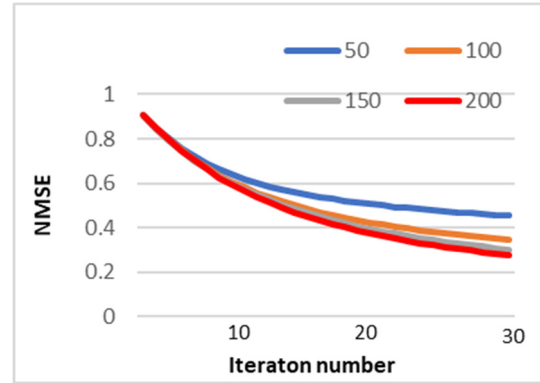


Figure 6: Plots of normalized mean square error versus iteration number. 200 detectors / view. Initial image is a uniform image of 1.0. Relaxation parameter is the unit. The number of views are changed from 50 to 200.

In this case, we set the number of detectors per view 200 and the relaxation parameter the unit. Initial data is a uniform image of 0.1, $0.1 = \mathbf{f}^0 \in \mathbb{R}^M$. From Fig. 6 we can see that the error decreases with increasing the number of iterations. From Fig. 5 and Fig. 6, it is more important that if the number of detectors, views and iterations can be increased, NMSE can be decreased.

3.3 Head Phantom

Our original test image 2 is 2-dimensional numerical phantom which is the well-known Shepp and Logan's head phantom and models cross section of the human head (Kak et al., 1998). This phantom is a superposition of 10 ellipses. Figure 7 shows its test image 2, discretized 128×128 pixels, 8 bit/pixel. Figure 8 shows the projection data of the original test image 2. The number of detectors per view is 200. The number of views per 360° is 200. Figure 9 shows the reconstructed images by ISRA. In this case, iteration number is 50. The number of detectors per view is 200. The number of views per 360° is 200. Initial data is a uniform image of 1.0, $1.0 = \mathbf{f}^0 \in \mathbb{R}^M$. The relaxation parameter is the unit.

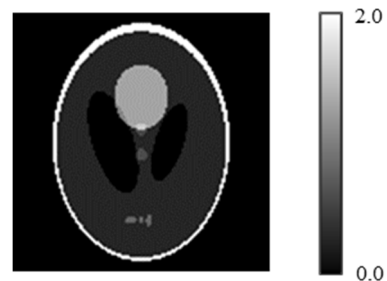


Figure 7: The original test image 2 (128×128 pixels, 8bpp).

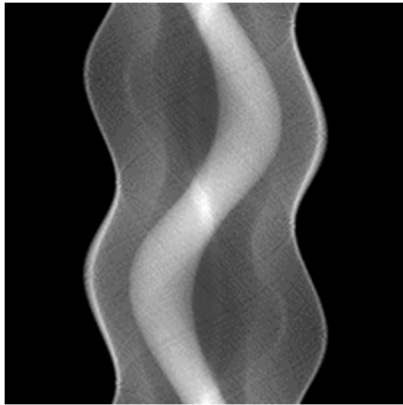


Figure 8: The projection data, Sinogram of the original image in Fig. 7. 200 detectors / view, 200 views / 2π and 8bpp. Noise free.

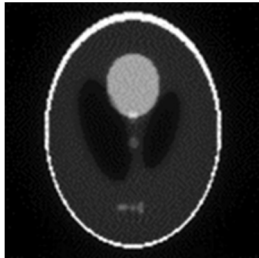


Figure 9: The reconstructed image by ISRA after 50 iterations. Initial image is a uniform image of 1.0. The relaxation parameter $\gamma_j = 1.0$.

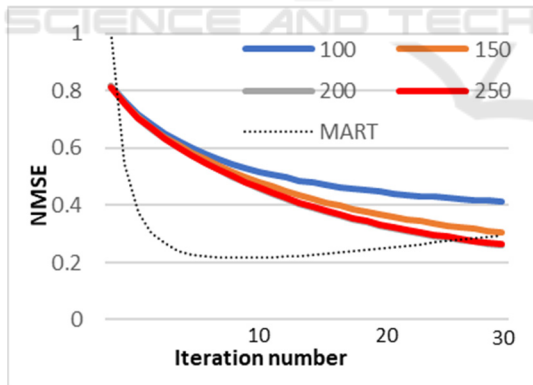


Figure 10: Plots of normalized mean square error versus iteration number. 200 views. Initial image is a uniform image of 1.0. Relaxation parameter is the unit. The number of detectors / view are changed from 100 to 250.

To confirm the effect of number of detectors per view, we computed the reconstructed image with its variations from 100 to 250. Figure 10 illustrates the plots of the normalized mean square error versus iteration number. In this case, we set the number of views per 360° 200 and the relaxation parameter the

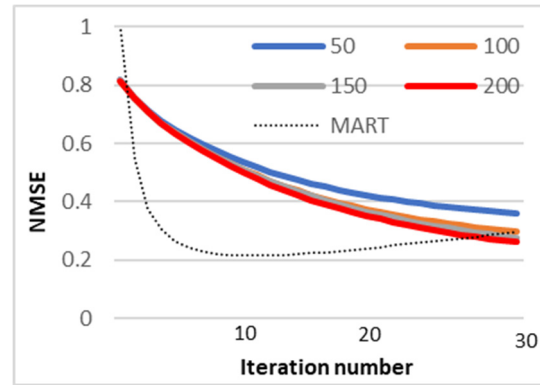


Figure 11: Plots of normalized mean square error versus iteration number. 200 detectors / view. Initial image is a uniform image of 1.0. Relaxation parameter is the unit. The number of views are changed from 50 to 200.

unit. Initial data is a uniform image of 1.0, $1.0 = \mathbf{f}^0 \in \mathbb{R}^M$. Iteration number is up to 30. We computed the reconstruction image of multiplicative algebraic reconstruction techniques (MART) in same conditions for reference (Aoyagi et al., 2020). MART which is updated by multiplication is similar in ISRA. We set the number of views 200, the number of detectors per view 200 and the relaxation parameter the unit. From Fig. 10 we can see that the error decreases with increasing the number of iterations and the error decreases as a whole with increasing the number of detectors. To confirm the effect of number of views per 360° , we computed the reconstructed image with its variations from 50 to 200. Figure 11 illustrates the plots of the normalized mean square error versus iteration number. In this case, we set the number of detectors per view 200 and the relaxation parameter the unit. Initial data is a uniform image of 1.0, $1.0 = \mathbf{f}^0 \in \mathbb{R}^M$. From Fig. 11 we can see that the error decreases with increasing the number of iterations. From Fig. 10 and Fig. 11, we have found that if the number of detectors, views and iterations can be increased, NMSE can be decreased.

To confirm the effect of relaxation parameter, we computed the reconstructed image with its variations from 0.6 to 1.4. Figure 12 illustrates the plots of the normalized mean square error versus relaxation parameter. In this case, we set detectors per view 200 and views per 360° 200. Initial data is a uniform image of 1.0, $1.0 = \mathbf{f}^0 \in \mathbb{R}^M$. Iteration number is up to 30. From Fig. 12 we can see that the error decreases with increasing the relaxation parameter. If the relaxation parameter is more than 1.4, we cannot confirm precisely whether NMSE decrease yet.

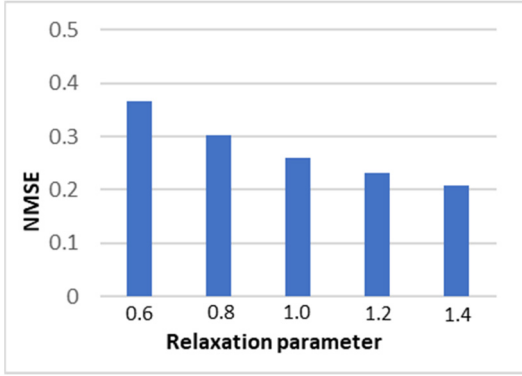


Figure 12: Plots of normalized mean square error versus relaxation parameter. 200 detectors / view. 200 views. Initial image is a uniform image of 1.0. Relaxation parameter is changed from 0.6 to 1.4. 30 iterations.

3.4 Weighting Factors

To confirm the effect of the weight w_i in eq. (8), we introduce the new weighting factor, such that,

$$w_i = \mu \mathbf{p}^k + \nu \mathbf{g} + \delta, \quad (14)$$

where μ, ν and δ are in \mathbb{R}^1 respectively. From eqs. (8) and (14), we obtain

$$\mathbf{f}_j^{k+1} = \mathbf{f}_j^k \frac{\sum_{i=1}^N a_{ij} \frac{\mathbf{g}_i}{\mu \mathbf{p}^k + \nu \mathbf{g} + \delta_1}}{\sum_{i=1}^N a_{ij} \frac{p_i^k}{\mu \mathbf{p}^k + \nu \mathbf{g} + \delta_2}}. \quad (15)$$

If the weighting factor are set as $w_i = p_i^k$, i.e. $\mu = 1, \nu = 0, \delta = 0$, then the well-known ML-EM algorithm is obtain, that is,

$$\mathbf{f}_j^{k+1} = \mathbf{f}_j^k \frac{\sum_{i=1}^N a_{ij} \frac{\mathbf{g}_i}{\mathbf{p}^k}}{\sum_{i=1}^N a_{ij} \frac{p_i^k}{\mathbf{p}^k}} = \frac{\mathbf{f}_j^k}{\sum_{i=1}^N a_{ij}} \sum_{i=1}^N a_{ij} \frac{\mathbf{g}_i}{p_j^k}. \quad (16)$$

In this case a_{ij} is the probability that a positron emitted from voxel j results in an event being registered in sinogram bin i . If the weighting factor are set as $w_i = 1$, i.e. $\mu = 0, \nu = 0, \delta = 1$, then standard ISRA is obtained.

Figure 13 illustrates the plots of the normalized mean square error versus iteration number. We computed three cases in eq. (15) and set the number of detectors per view 200, the number of views per 360° 200, and the relaxation parameter the unit. Initial data is a uniform image of 1.0, $1.0 = \mathbf{f}^0 \in \mathbb{R}^M$. The blue line is NMSE at $\mu = 0, \nu = 0, \delta = 1$, that is, $w_i = 1.0$. The orange line is at $\mu = 0.5, \nu = 0, \delta = 0$, that is, $w_i = 0.5 \times \mathbf{p}^k$. The red line is at $\mu = 0, \nu = 0.5, \delta = 0$, that is, $w_i = 0.5 \times \mathbf{g}$. From Fig. 13 we can see that the method which have some weighting

factors are slightly better than standard ISRA. Changing the range of μ from 2.0 to 0.05, there was no influence in NMSE.

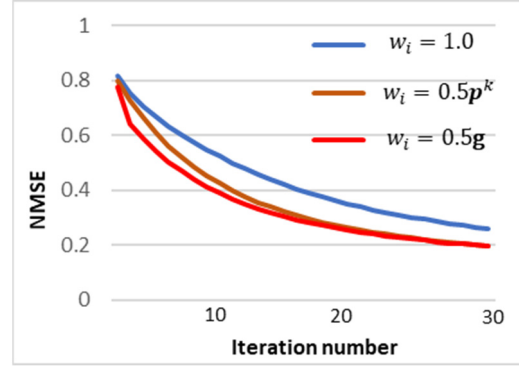


Figure 13: Plots of normalized mean square error versus iteration number. 200 detectors/view. 200 views/ 2π . Initial image is a uniform image of 1.0. Relaxation parameter is the unit. The weight is changed.

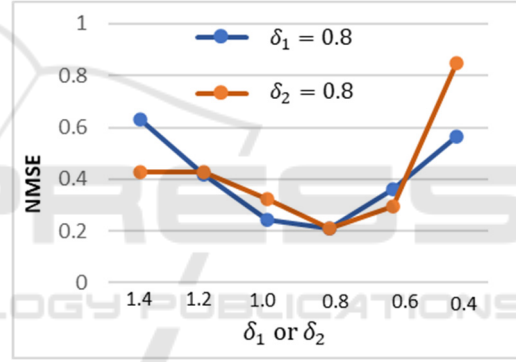


Figure 14: Plot of the normalized mean square error versus δ . 200 detectors/view. 200 views/ 2π . Initial image is a uniform image of 1.0. Relaxation parameter is 1.4.

Figure 14 illustrates the plots of the normalized mean square error versus δ_1 and δ_2 . The blue line is NMSE in $\delta_2 \in [1.4, 0.4]$ if δ_1 was fixed at 0.8. The orange line is NMSE in $\delta_1 \in [1.4, 0.4]$ if δ_2 was fixed at 0.8. From Fig. 14 we can see that NMSE is the smallest if both δ_1 and δ_2 was fixed at 0.8.

3.5 Noise Effects

To confirm the effect of the noise, gaussian noises are added to the projection data. Using vector notation, it can be expressed by

$$\mathbf{g} = \mathbf{A}\mathbf{f} + \mathbf{q}, \quad (17)$$

where \mathbf{q} indicates noise and is a normally distributed deviate with zero mean and unit variance (Press et al., 1992). To measure the effect of noise on the reconstruction images, we use the signal-to-noise

ratio (SNR) (Trussel, 2008). This is usually defined as the ratio of signal power σ_g^2 , to noise power σ_q^2 ,

$$\text{SNR} = \frac{\sigma_g^2}{\sigma_q^2}, \quad (18)$$

and in decibels

$$\text{SNR}_{\text{dB}} = 10 \times \log_{10} \left(\frac{\sigma_g^2}{\sigma_q^2} \right). \quad (19)$$

In projection data, the function power is usually estimated by the simple summation

$$\sigma_g^2 = \frac{1}{N} \sum_{i=1}^N \{g_i - \mu_g\}^2, \quad (20)$$

where μ_g is the mean of the projection data.

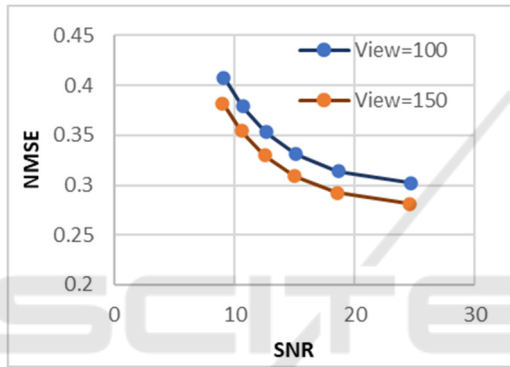


Figure 15: Plot of the normalized mean square error versus SNR. 200 detectors/view. Initial data is a uniform image of 1.0. Iteration number is 30. The number of views/ 2π are changed from 100 to 150.

Figure 15 illustrates the plots of the normalized mean square error versus SNR. From Fig. 15 we can see that the error decreases with increasing SNR and the error decreases with increasing the number of views.

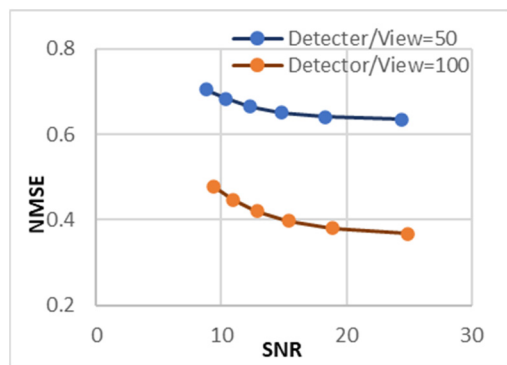


Figure 16: Plot of the normalized mean square error versus SNR. 150 views/ 2π . Initial data is a uniform image of 1.0. Iteration number is 30. The number of detectors/view are changed from 50 to 100.

Figure 16 illustrates the plots of the normalized mean square error versus SNR. From Fig. 16 we can see that the error decreases with increasing SNR and the error decreases with increasing the number of detectors/view.

4 CONCLUSIONS

By discretizing the image reconstruction problem, we applied ISRA to the problem and evaluated the image quality. We showed that the error decreases with increasing the number of detectors, views and iterations. Also, we showed the effect of the relaxation parameter and noise to the reconstructed image.

We confirmed that the number of views, detectors-source pair, relaxation parameters, iteration numbers and weighting factors influenced the quality of the reconstructed image. The size of system matrices which were defined by detectors and views was changed. If the size and iteration number was large, computation of our algorithm consumed time to large quantities. It is necessary to reveal the optimal parameter of relaxation. By modifying the weighting factors for the method of steepest descent, it is possible to produce the new update methods. It is important to evaluate the new methods.

REFERENCES

- Herman, G. (2009). Fundamentals of Computerized Tomography, 2nd edition, Springer-Verlag London.
- Kak, A., Slaney, M. (1988). Principles of computerized tomographic imaging, IEEE Press, New York.
- Imiya, A. (1985) A direct method of three-dimensional image reconstruction from incomplete projection, Dr. Thesis, Tokyo Institute of Technology, Tokyo. [Japanese]
- Bendriem, B., Townsend, D. (1998). The theory and practice of 3D PET, Kluwer Academic Publishers, Dordrecht.
- Stark, H. (1987). Image Recovery: theory and application, Academic Press, New York.
- Natterer, F., Wubbeling, F. (2001). Mathematical Methods in Image Reconstruction, SIAM, Philadelphia.
- Daniel, G. (2021) A new interpretation of (Tikhonov) regularization, Inverse Problems, 37(6), 064002.
- Ronny, R., Lothar R. (2019) Error estimates for Arnoldi–Tikhonov regularization for ill-posed operator equations, Inverse Problems, 35, 055002.
- Simon, H., Ronny, R., Lukas W. (2022) On regularization via frame decompositions with applications in tomography, Inverse Problems, 38, 055003.

- Depierro, A. (1987). On the convergence of the iterative image space reconstruction algorithm for volume ECT, *IEEE trans. Med. Imaging*, 6(2), 174-175.
- Iniyatharasi, P., Pallikonda, M., Arun, T., Kannan, S. (2015) PET image reconstruction using ISRA technique, *Australian J. Basic and Applied Sciences*, 9(16), 110-117.
- Depierro, A. (1993) On the relation between the ISRA and the EM algorithm for positron emission tomography, *IEEE trans. Med. Imaging*, 12(2), 328-333.
- Reader, A., Letourneau, E., Verhaeghe, J. (2011) Generalization of the image space reconstruction algorithm, *IEEE Nucl. Sci. Symp. Conf. Record*. 4233-4238.
- Bertero, M., Mol, C., Pike, E. (1985), Linear inverse problems with discrete data. I: general formulation and singular system analysis, *Inverse Problems*, 1, 301-330.
- Bertero, M., Mol, C., Pike, E. (1988), Linear inverse problems with discrete data: II: stability and regularization, *Inverse Problems*, 4, 573-594.
- Luenberger, D. (1969). *Optimization by vector space methods*, John Wiley & Sons. New York.
- Luenberger, D. (2003). *Linear and nonlinear programming*, Kluwer Academic Publishers. Boston, 2nd edition.
- Censor, Y., Elfving, T., Herman, G., Nikazad, T. (2008). On diagonally-relaxed orthogonal projection methods. *SIAM J. Sci. Comput.* 30, 473-504.
- Press, W., Teukolsky, S., Vetterling, W., Flannery, B. (1992). *Numerical Recipes in C*, Cambridge University Press. Cambridge, 2nd edition.
- Aoyagi, T., Ohtsubo, K., Aoyagi, N. (2020) Implementation and numerical evaluation for multiplicative algebraic reconstruction techniques, *OPTICS & PHOTONICS International Congress 2020(The 6th Biomedical Imaging and Sensing Conference)*.
- Trussel, H., Vrhel, M. (2008). *Fundamentals of Digital Imaging*, Cambridge University Press. Cambridge.